

## ENHANCED PERMEABILITY ESTIMATION IN NON-CORED WELLS USING A MODIFIED FLOW ZONE INDEX-PERMEABILITY CROSSPLOT: A CASE STUDY OF CARBONATE RESERVOIRS

Usama Alameedy\*<sup>1</sup>, Ali Rabia<sup>2</sup>, Hawraa Hamid<sup>1</sup>

<sup>1</sup>College of Petroleum Engineering, University of Baghdad, Baghdad, Iraq

<sup>2</sup>Wireline Logging Department, COSL Middle East Iraq Branch, Baghdad, Iraq

### ABSTRACT

The permeability estimates for the uncored wells and a porosity function adopting a modified flow zone index-permeability crossplot are given in this work. The issues with implementing that approach were mostly crossplots, due to the influence of geological heterogeneity, did not show a clear connection (scatter data). Carbonate reservoir flow units may now be identified and characterized using a new approach, which has been formally confirmed. Due to the comparable distribution and flow of clastic and carbonate rock fluids, this zoning method is most effective for reservoirs with significant primary and secondary porosity. The equations and correlations here are more generalizable since they connect these variables by combining core analysis with log data. The cross-sectional parts of the reservoir are examined in seven zones. The result demonstrates a better connection between this crossplot and traditional crossplot and a more straightforward transformation to estimate permeability in an uncored well to input models for geological and reservoir simulation and six hydraulic flow zones in the field for four wells. Start with this conception; we try to simplify the parameter  $S_{wir}$  correlation with the Carmen-Kozeny equation, which varies across flow units but remains constant within each unit; it is added as another parameter influencing permeability. Future full-field simulation models will benefit significantly from this improved permeability estimate, leading to more accurate and reliable performance predictions.

**Keywords:** flow zone indicator; hydraulic flow unit, permeability; reservoir quality index; multi-resolution graph-based clustering.

**Date submitted:** 26.02.2025

**Date accepted:** 06.05.2025

© 2025 «OilGasScientificResearchProject» Institute. All rights reserved.

### 1. Introduction

Traditional rock typing methods use simple regression to assess permeability based on log-derived porosity measurements. It's common to see a straight line between the two properties of a log, however, this doesn't hold for carbonate formation [1]. The porosity is typically plotted on the x-axis as a fraction, while the permeability is plotted on the y-axis in millidarcy (md) [2]. Figure 1 demonstrates the relationship between permeability and porosity for four wells of core samples taken from a carbonate deposit. Although permeability and porosity have a weak correlation ( $R_2=0.37$ ), the scattering results show that this formation is nonuniform and heterogeneous, and the link between permeability and porosity is purely qualitative, rather than quantitative in any manner. In the next part, a case study will examine how the permeability of this sort of carbonate system relates to other petrophysical parameters.

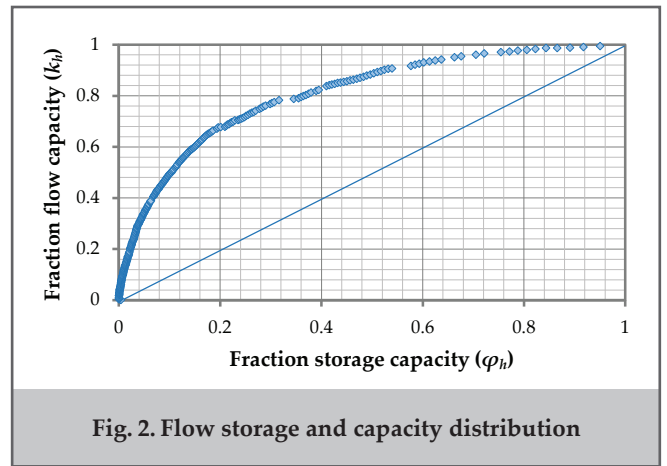
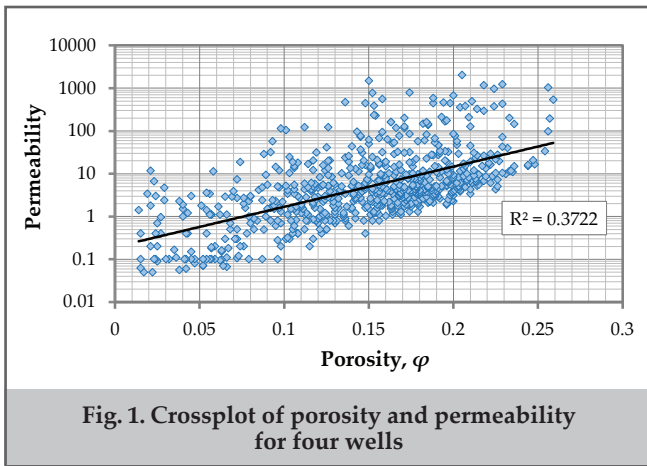
Using information on the capillary pressure created by injecting mercury into a sample, [3] derived an empirical

equation connecting porosity, permeability, and pore aperture. There were 240 samples without their permeabilities corrected and 82 samples with low permeabilities due to gas slippage in his data set (56 sandstone and 26 carbonate). Using the help of multiple regression analysis, he determined that the sample mercury saturation of 35% was the best representation of the modal pore aperture radius. [4] increased the number of samples that Winland originally used, improved the process for selecting the dominant pore aperture, and modified the Winland equation.

As a carbonate specialist in 1999, Lucia [5] observed that finer grains and fabrics were more prevalent in the cross plots' south-eastern part while coarser grains and fabrics were more prevalent in the plot's north-western section. Although Lucia worked with carbonates, the main ideas also hold for clastic. A lower rock fabric number (RFN) indicates a rock with a coarser grain, whereas a higher RFN indicates a rock with a finer grain.

Rock typing is a crucial step in reservoir characterization and modeling. It involves identifying groups of rocks that have similar geological, fluid flow, and reservoir properties based on available data related to rock characteristics,

\*E-mail: Usama.sahib@coeng.uobaghdad.edu.iq  
<http://dx.doi.org/10.5510/OGP20250201067>



such as lithology, porosity, and permeability [6]. The goal is to establish rock types that are internally homogeneous and externally distinct, which can then be used to estimate unknown reservoir parameters in each grid cell. Depending on the data available and the goals of the reservoir study, different ways of classifying rocks can be used [7-10] proposed a method that integrates different evaluations of rock typing at different scales, including depositional, petrographic, and hydraulic. This method involves analyzing drilling core data to identify key lithofacies and rock types, and then using petrophysical and hydraulic measurements to characterize the porosity, permeability, and other relevant properties of each rock type. Other common rock-typing methods include statistical clustering, principal component analysis, and expert-based classification. Statistical clustering involves grouping rocks based on their similarity in terms of multiple rock properties, while principal component analysis identifies the dominant factors that control reservoir properties and groups rocks based on these factors [8, 11]. The expert-based classification relies on geological and petrophysical expertise to define rock types based on lithology, texture, mineralogy, and other characteristics.

**2. Data and methods**

Units were defined by geologists and engineers from the description of reservoir zones as storage containers and fluid pathways in reservoirs. Flow units, according to the study, are the result of the depositional environment and the diagenetic process. The hydraulic (pore geometrical) unit represents the entire reservoir rock’s fundamental volume from the standpoint of geology and petrophysics [12]. As compared to other reservoir rock volume characteristics, hydraulic flow units are a continuous and predictable component of the reservoir where geological and petrophysical factors affect fluid flow [13]. There are two types of flow units, one having the properties of permeability, porosity, and bedding, which is what [14] term a «flow unit». The following definition of a continuous stratigraphical interval is used [15].

Dykstra-Parsons permeability variation ( $V_K$ ) and the Lorenz coefficient ( $L_K$ ) are two measures of spatial heterogeneity used in geostatistics to describe the distribution of reservoir parameters such as porosity and permeability.  $V_K$  is a dimensionless parameter that quantifies the degree of permeability variation within a sample, while  $L_K$  is a dimensionless parameter that measures the degree of heterogeneity in a sample based on the statistical distribution of the sample’s

values. Both  $V_K$  and  $L_K$  can help predict how a reservoir will work and manage hydrocarbon reservoirs by giving useful information.

**2.1. Reservoir heterogeneity assessment**

*2.1.1. Lorenz coefficient ( $L_K$ )*

For the permeability distribution, [16] created the Lorenz coefficient, which is known today as the  $L_K$ . The relationship indicated in (fig. 2) may be obtained by graphing the storage capacity ( $k$ ) against the flow capacity ( $k_h$ ).  $L_K$  has a value between 0 and 1. If  $L_K=0$ , the reservoir’s permeability distribution is deemed uniform [17]. If  $L_K=1$ , the reservoir is thought to be heterogeneous. The reservoir is largely heterogeneous based on the present data, which is  $L_K=0.86$ . Multiple permeability distributions may give the same  $L_K$  value; thus, this coefficient is not specific to a particular reservoir.

*2.1.2. Reservoir heterogeneity index*

Variation in Dykstra Parsons permeability the reservoir heterogeneity index (RHI) is another name for  $V_K$ . In terms of sample variability or dispersion, it has no dimensions [18]. It’s the sample standard deviation to the sample mean as a ratio. Permeability heterogeneity is frequently assessed using  $V_K$  in Geoscience engineering investigations [19].

$$V_K = 1 - \exp \left[ -\sqrt{\ln \left( \frac{k_a}{k_h} \right)} \right] \tag{1}$$

where  $k_a$  represents the average permeability and  $k_h$  represents the horizontal permeability. For an ideal, homogeneous reservoir, the reservoir heterogeneity index value is 0, and for a more realistic, heterogeneous reservoir, the index value is between 0.25 and 0.50. For a reservoir that is more realistically heterogeneous, the index value is 0.50-0.75, and for one that is truly heterogeneous, the index value is less than 0.75 and greater than 1, which corresponds to a perfectly heterogeneous reservoir. Because geologic processes of sediment deposition and accumulation are not severe, it is doubtful that such reservoirs exist [20]. Applying this technique found the  $V_K \approx 1$  (standard deviation equation), and  $V_K=0.72$  this vibration indicates the heterogeneity range from very heterogeneous to extremely heterogeneous.

**2.2. Characterization of flow unit approaches**

A practical method of reservoir zonation is to divide a carbonate reservoir into flow units. The existence of discrete units with unique petrophysical properties such as porosity,

permeability, water saturation, and pore researches allow for the establishment of a robust reservoir characterization. Once the flow unit determination is made, it's easier to predict how a reservoir will behave over time. Hydrocarbon storage and flow capacity both influence the quality and future performance of a reservoir. These aid in the definition of intervals with comparable and predictable flow properties, which are referred to as flow units in this context. The word flow unit was first used to characterize the correlation units found in reservoirs, and it has since been more widely used [7]. A flow unit (also known as a hydraulic flow unit) is defined as the typical elementary volume of total reservoir rock within which geological and petrophysical characteristics that influence fluid flow are internally consistent and predictably distinct from the properties of other rock volumes. [14] and [21] came up with the term «Flow Unit» to define geological units within a stratigraphic framework that have petrophysical characteristics that fall within specified ranges.

The reservoir quality index (RQI), which considers the pore, grain distribution, pore-throat, and grain distribution, as well as other macroscopic characteristics, was proposed by [21]. Equation (2) denotes the reservoir's quality index as follows:

$$RQI = 0.0314 \frac{\sqrt{\frac{k}{\phi}}}{\left(\frac{\phi}{1-\phi}\right)} \quad (2)$$

Using millidarcies as a unit of permeability and a fraction as a measure of porosity, the left side of Equation (2) may be rewritten as  $FZI = 0.0314 \sqrt{\frac{k}{\phi}}$ , and  $\phi_z = \left(\frac{\phi}{1-\phi}\right)$  before applying the logarithm to both sides to arrive at:

$$\log(RQI) = \log(\phi_z) + \log(FZI) \quad (3)$$

When plotting RQI against z using Equation (3), a straight line with a unit slope result. The FZI is the point where this straight line meets a z=1 point. There will be several parallel lines of samples with varying FZI levels. Flow units are made up of samples that are all in the same straight line and have comparable pore throat properties. Clean limestone formations tend to have perfectly straight slopes. Shaly formations are found when there is a slope greater than one.

In addition to the definition of RQI, the following helpful equation provides a beneficial connection between RQI and FFI:

$$RQI = 3.14 \left(\frac{FFI}{\phi - FFI}\right) \sqrt{\phi^3} \quad (4)$$

where  $FFI = \phi (1 - S_{wir})$  and porosity are given as fractions, permeability is stated in millimeters per second, and RQI is expressed in micrometers per second. Taking the logarithm of both sides of Equation (5) results in the following result:

$$\begin{aligned} \log RQI &= \log\left(\sqrt{\phi^3}\right) + \log\left(\frac{3.14FF}{\phi - FF}\right) = \\ &= \log\left(\sqrt{\phi^3}\right) + \log(I_F) \end{aligned} \quad (5)$$

The Reservoir Quality Index (RQI) is a measure of the quality of a reservoir rock that considers both porosity ( $\phi$ ) and permeability ( $k$ ). The RQI is commonly plotted against the square root of the cube of porosity ( $\sqrt{\phi^3}$ ) on a log-log

scale. In a clean, homogeneous carbonate deposit, the RQI should have a slope of unity on this plot, indicating that the rock's permeability is directly proportional to the cube of its porosity. The intercept of the RQI at  $\sqrt{\phi^3} = 1$ , known as the Intercept Factor (IF), can also be used as a measure of the rock's pore-throat properties, irreducible water saturation and, in general, the flow unit characteristics. Create a correlation like that found in the [22] equation, which can then be generalized in the manner described below:

$$k = 10^{C_{cd}} \phi^4 \left(\frac{FFI}{\phi - FFI}\right)^2 \quad (6)$$

where  $C_{cd}$  is a correlation constant that is specific to the subject reservoir, it's reasonable to expect that different  $C_{cd}$  values may be obtained for clay-rich formations compared to clean formations, as the presence of clay can significantly affect the rock's pore structure and permeability. This correlation constant can be used to adjust the equation's coefficients for the specific reservoir rock type and mineralogy. However, it's important to have enough data to perform the regression analysis and to check the correlation coefficient and the residuals to ensure the goodness of fit. It may be beneficial to develop a relationship between this parameter and the shale fraction  $V_{sh}$ .

$$C_{cd} = \log\left(\frac{C_{pp}}{0.0314}\right)^2 \quad (7)$$

In this equation,  $C_{pp}$  denotes the permeability-porosity correlation coefficient. As previously discussed, if  $S_{wir}$  is known from capillary pressure measurements or well logs and the intercept IF is determined as discussed above, then  $C_{pp}$  can be calculated from the following equations:

$$C_{pp} = I_F \left(\frac{\bar{\phi}}{FFI} - 1\right) \quad (8)$$

$C_{pp}$  is an unmeasured quantity that is only useful for making comparisons between rocks of the same type or mineralogy; it may not be transferable to other reservoir rocks or even to different regions within the same reservoir. Keep in mind that the assumptions upon which this correlation is based, such as the rock being homogeneous and isotropic, may not hold in all situations, and proceed with caution when trying to apply the results of this equation to the real world.

Winland  $R_{35}$  charts [3], on the other hand, are charts that show the expected permeability of a rock sample for a given porosity and pore aperture radius ( $R_{35}$ ). The  $R_{35}$  is the average size of the pores in the rock sample. Winland found that the  $R_{35}$  was best shown when the samples were saturated with 35% mercury. By overlaying the Winland  $R_{35}$  charts onto the permeability vs. porosity plot, it becomes possible to estimate the expected permeability of a rock sample or reservoir rock based on its porosity and modal pore aperture radius. This can be useful in reservoir characterization and exploration, as it provides a quick way to estimate the potential production capabilities of a given reservoir rock. The Winland  $R_{35}$  charts can be adjusted in the Winland Pittman field in the controls panel at the top of the view to match the desired pore aperture radius for the analysis. Using multiple regression analysis, he determined that the point of 35% mercury saturation of the samples best represented the modal pore aperture radius. Winland created the following formula:

$$\log(R_{35}) = 0.732 + 0.588 \times \log(k) - 0.864 \times \log(\varphi) \quad (9)$$

The permeability and porosity are at ambient conditions. In the initial equation,  $\varphi$  is a percentage rather than a fraction (the input log for porosity is fractional, so it is multiplied by 100 to conform to the original equation). The modal pore throat radius, « $r$ », is measured in microns. Because the method relies on mercury injection, which calls for the removal of all water (including water that has been bound to clay), it is possible to infer that the input porosity is total porosity.

Pittman [4] built on Winland’s work by increasing the number of samples used in the analysis, improving the way the dominant pore aperture was chosen, and making changes to the Winland equation so that it better reflected the data. Pittman’s equation is:

$$\log(R_{35}) = A + B \times \log(k_{air}) - C \times \log(\varphi) \quad (10)$$

where  $k$  is the permeability in millidarcy (md),  $\phi$  is the porosity as a fraction,  $R$  is the modal pore aperture radius in microns, and  $A$ ,  $B$ , and  $C$  are fitting parameters that can be found through regression analysis. Pittman also noted that if sufficient core analysis and mercury injection data are available, it is encouraged to develop  $R_{35}$  (or another mercury percentage) equations specific to the particular area. The Pittman equations can be varied by choosing the mercury saturation value from the Chart Contours menu. The most common mercury saturation value used is  $R_{35}$ . The data that are available and the regression analysis used to fit the equation determines the different mercury saturation values that can be chosen for each equation. By choosing the right mercury saturation value, you can use the porosity and modal pore aperture radius of a rock sample or reservoir rock to estimate its permeability. This can help with reservoir characterization and exploration because it gives a quick way to estimate how much oil or gas a certain reservoir rock might be able to produce.

Lucia [5] researched carbonate rocks that showed that grain size, fabric, and permeability are all linked. He found that coarse-grained rocks and fabrics were more likely to be found in the northwestern part of a log-log porosity-permeability crossplot, while fine-grained rocks and fabrics were more likely to be found in the southeast part of the crossplot. Lucia’s approach was different from those of Winland, Pittman, and Amaefule because he focused on the relationship between grain size and fabric rather than pore throat radii. Instead of pore throat radii, the lines on Lucia’s crossplot are based on the size of the grains in the rocks. This division is often more directly related to the core sedimentary facies or the physical features of the sedimentary environment where the rock formed. Lucia’s work on carbonate rocks is also useful for clastic rocks because the general rules about how grain size and fabric affect permeability apply to all types of rocks. Overall, Lucia’s research helps us learn more about the complicated relationship between rock properties and permeability. It also shows how important it is to think about both grain size and fabric when judging reservoir rocks. Lucia’s way of grouping rocks is based on the rock fabric number (RFN), which measures how well the grains inside a rock are sorted and packed. The size, shape, and arrangement of the grains within the rock are considered when calculating RFN using thin-section pictures of the rock. Rocks with coarser grains and poorer packing have lower

RFNs, while rocks with finer grains and better packing have higher RFNs. Lucia’s equation is:

$$\log k = A - B \times \log(RFN) + (C - D \times \log(RFN)) \times \log(\varphi) \quad (11)$$

where:  $k$  is permeability in md log is to base 10,  $A=9.7982$ ,  $B=12.0838$ ,  $C=8.6711$ ,  $D=8.2965$ , RFN rock fabric number, and  $\varphi$ =effective porosity (clay bound water removed, but capillary bound water in fines remaining)

### 2.3 Machine learning (ML)

Using geoscientific techniques helps one to better understand the formation, fluid composition, and most efficient way to remove that composition from a reservoir. Considered are fluid storage capacity, petrophysical properties, and reservoir capacity to move these fluids to the wellhead [23]. Reservoir characterization provides a complete knowledge of the formation required for an effective oil recovery strategy by incorporating exploration, drilling, reservoir management, production, and final field abandonment. In the oil and gas industry [24], ML is becoming more and more important for future production prediction, formation assessment, drilling operations design, reservoir characterization, and production stimulation characterization [25]. The quantitative study of the permeability, porosity, and other petrological features of rocks may be helped by machine learning. Using SVR, RBF, and MLP modules clusters the dataset such that machine learning methods including artificial neural networks may estimate permeability values from many well-logging data and core measurements. developed a hybrid method to improve permeability estimate accuracy by combining MRGC with rock type approaches. Integration of the three rock-typing techniques into multi-resolution graph-based clustering (MRGC) yields the permeability of a rock [26]. As show in figure 3 almost half of the correlation from the Coates equation comes from the clustering approach.

#### 2.3.1. Electrofacies and clustering

A series of log responses called electrofacies defines a deposit and helps one rock type to be identified from another. One broad class of facies, rock types, or clusters produced or decided upon by log processes is electrofacies [27]. In machine learning, clustering is a technique for partitioning vast volumes of data into smaller, more reasonable pieces. One might break apart a set of data points into distinct groups using a clustering method. While data points from various groups should vary greatly, generally data points from the same group should have similar quality and/or

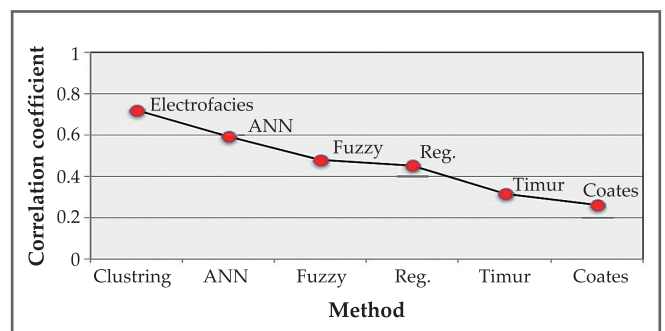


Fig. 3. Prediction of permeability using correlation against the method used

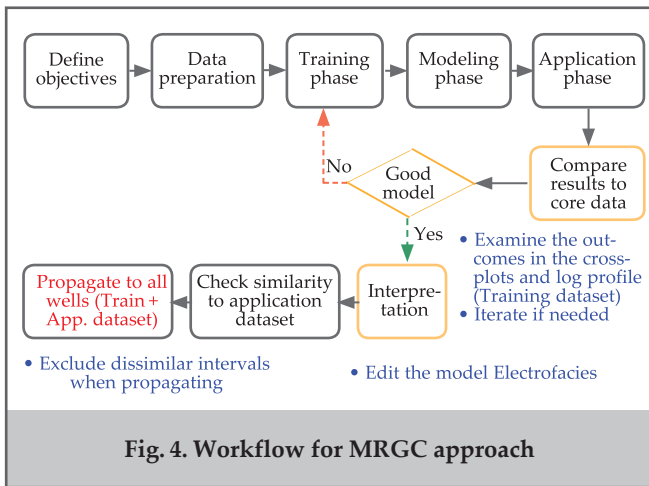


Fig. 4. Workflow for MRGC approach

traits. In statistical data analysis, clustering is a somewhat popular unsupervised learning method. The interconnection of the modeling process is shown by the application of log predictions and electrofacies [28]. It is imperative to query and respond to the interval that has to be managed before using the electrofacies workflow diagram and log-predict modeling technique. The issue is «Which wells should one consider while deciding the reference wells?» by means of individual inspections of every pair of logs, one may identify specific rock characteristics like sedimentation, diagenesis, and pore network activity [29]. Different log combinations so expose the many aspects of the rock. The gold standard is a benchmark comprising considerable geological data, log and core cross-validation, and the whole log suite. For every discrete age of interest in the stratigraphic record or fluid zone, individual models are developed. The values of every imaginable log combination change uniformly. Different log pairings might point to sedimentation, diagenesis, activity of a porous network, and other rock properties [30]. There is no reason to reject anticipated core measurements as input logs if the fundamental data used to build the prediction model is representative. During the training phase, this project consists of creating a methodical approach for gathering and recognizing core samples as well as measuring their dimensions. Analyzing if the model can separate log responses into pertinent electrodes comes next to cluster similarity and neural network analysis of the training data, one may switch between models at any time throughout the modeling process. To get a good match, this calibration process has to be finished many times as show in (fig. 4).

Getting a functional ML model validated comes last in the process of producing one. This is accomplished by feeding the model data not used during the training phase to observe whether it can generalize or if it just learned the traits found in the training data. Should the model show good performance on the validation set, it is said to be «real-world ready» [31]. One could investigate other error measures to assess the generalizing capability of the model [32].

### 2.3.2. Minimum error and T-tests

Methodical studies both have statistical test values; one of them is the t-value extensively applied in statistics. One must do a null hypothesis test whereby the means of the two test samples exactly line up. Should the means of a t-test or regression analysis show contradicting results, the researchers will reject the null hypothesis and embrace the alternative

hypothesis. The test results show the resemblance between the two samples and the importance of the difference between the anticipated and observed mean permeability depending on the following computation.

$$t = \frac{(\bar{x} - \mu_0)}{s / \sqrt{n}} \quad (12)$$

Where,  $\bar{x}$  the average,  $\mu_0$  of all the samples;  $s$  is the standard deviation;  $n$  is the overall data size. Data prediction calls for a characterization of the interaction between the computed and observed variables. Determining the expected log value is made possible by aggregating the log values of several members and giving weights based on their membership condition. Often used numerical equations 13 and 14, respectively, in several disciplines to assess the accuracy of forecasts are the mean absolute error (MAE) and the root mean squared error (RMSE). Optimal models are selected depending on their capacity to forecast values with the lowest possible error.

$$RMSE = \sqrt{\frac{\sum (y_i - y_p)^2}{n}} \quad (13)$$

$$MAE = \frac{|(y_i - y_p)|}{n} \quad (14)$$

where  $y_i$  for a measured sample, this is actual;  $y_p$  is computed as permeability.

## 3. Results and analysis

The X formation in the study field was subjected to the hydraulic unit (HU) technique, which collected core data from five wells (well 1, well 2, well 3, well 4, well 5). A plot of RQI vs z is shown in (fig. 5a). Samples that lie on the same straight line together form a hydraulic unit, and the analysis identified seven different HU with variable numbers of HU. The correlations for the FZI are obtained using Equation 9 and (fig. 5a) and tabulated in table 1, which were used to define these HUs. Figure 5b depicts the comparable plot of horizontal permeability vs porosity each pore.

Geometrical facies have its texture and mineralogy, which are integrated into one parameter in the FZI. Because of their high surface area, tortuosity, fine-grained nature of the sand they are composed of, and the insufficient sorting procedure used to form them, HU-6 and Hu-5 have a low FZI index (fig. 5a). In comparison, tiny surface areas with low formation factors and tortuosity result in high FZI values, such as HU-1 and Hu-2, as shown in (fig. 6). These characteristics are confirmed when clean limestone exists that is less shaly, coarse-grained, and well-sorted. Depositional conditions and diagenetic processes influence the reservoir's shape and, therefore, the flow zone index.

It is important to note that the use of FZI in reservoir simulation models should be done with caution, as it is not a directly measurable physical property of the rock and its accuracy relies on the quality of the input data used to calculate it. Furthermore, the relationship between FZI and log measurements may not hold for all reservoirs and rock types. Therefore, it is recommended to use a combination of different rock typing methods and calibration with well data to ensure the accuracy of permeability estimation in reservoir simulation models. Figure 6 illustrates a comparable representation of the horizontal permeability versus porosity

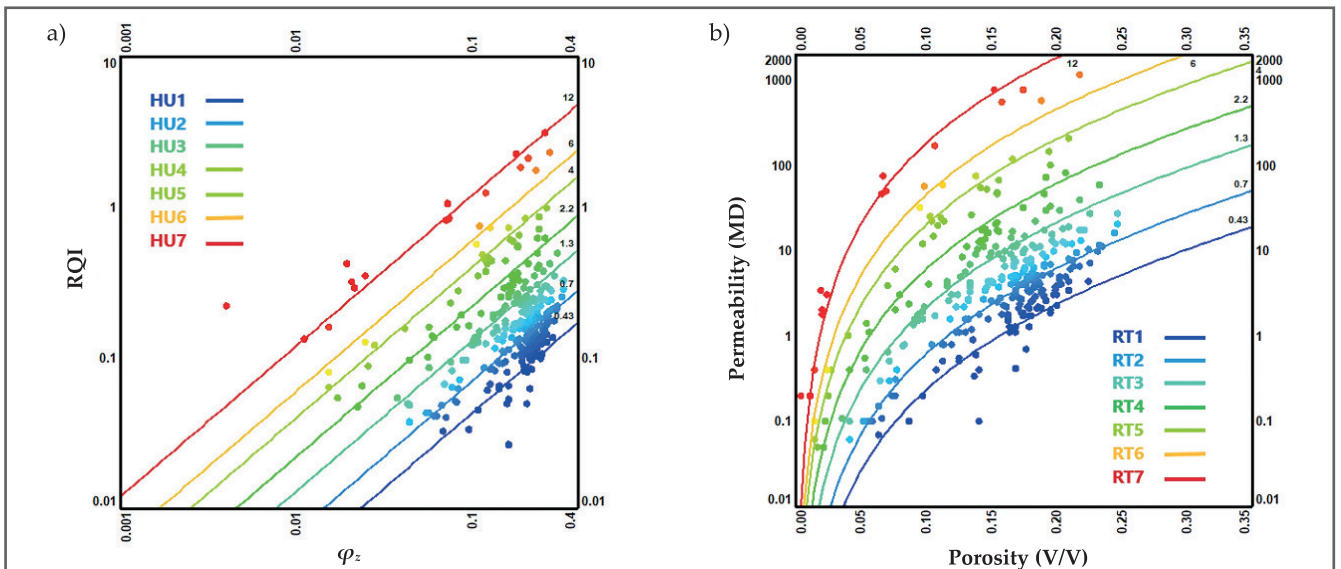


Fig. 5. a) RQI vs  $\phi_z$ , b) permeability vs. porosity for 5 wells and X1, X2, and X3 units

plot. Furthermore, the Winland  $R_{35}$  method utilizes Eq. 10 to determine the rock types.

Figure 7a shows a plot of horizontal air permeability versus porosity for the formation mentioned, along with straight lines that show  $R_{35}$  (microns) for each rock type listed. Based on the Winland  $R_{35}$  rock typing concept, you can separate seven different groups of data. Figure 7b shows the Pittman method, which was an improvement on Winland’s method because it used more samples and made it easier to pick the one with the most pores. Pittman also modified the Winland equation, as depicted in Eq. 10. The resulting formula is presented in table 2 for reference.

For all of the X1, X2, and X3 units, figure 7 depicts semi-log scale permeability vs. porosity using Lucia trends created from equation 11. In the X1 unit, the limestone is made of tiny skeletal pieces, including benthonic foraminifera, pelagic foraminifera, and echinoderms. Grainy samples show a range of RFN from 0.01 to 2. A well-sorted, fine- to medium-grained skeleton washstone or packstone makes up the majority of the X2 unit (RFN from 0.02 to 2.5), with grainstone and mudstone serving as supporting components. Benthonic foraminifera predominate in the limestone, and clay, silt, and very fine-grained sandstone make up the interbedded shale. Due to its low porosity and permeability, it is not seen as a large reservoir. Three subunits make up the X3 unit (RFN from 0.8 to 3.4), known as X3a, X3b, and X3c. The highest component, X3a, is primarily made up of wackestone and grainstone that are ooidal and poloidal. The middle subunit, X3b, is made up of limestone embedded in marl. The marl is made up of clay, silt, and very fine-grained sandstone. The limestone, on the other hand, is made up of bioclastic packstone or wackestone, with grainstone below it. The lowest subunit, X3c, is composed of limestone with interspersed shale. The shale is made up of clay, silt, and very fine-grained sandstone, whereas the limestone is made up of bioclastic wackestone or packstone with subordinate grainstone. Table 3 summarizes the Lucia rock type and RFN ranges from (fig. 8) and Eq. 11.

These rock types are extremely diverse, and a single model might not be able to adequately capture the significant differences in grain and pore size that result from a variety of

Rock type	Range of FZI	FZI Average	$k-\phi$ formula
RT1	FZI>0.34	0.43	$k = 1014 \times (0.43)^2 \frac{\phi^3}{(1-\phi)^2}$
RT2	0.34 ≤ FZI < 0.75	0.7	$k = 1014 \times (0.7)^2 \frac{\phi^3}{(1-\phi)^2}$
RT3	0.75 ≤ FZI < 1.5	1.3	$k = 1014 \times (1.3)^2 \frac{\phi^3}{(1-\phi)^2}$
RT4	1.5 ≤ FZI < 2.94	2.2	$k = 1014 \times (2.2)^2 \frac{\phi^3}{(1-\phi)^2}$
RT5	2.94 ≤ FZI < 5	4	$k = 1014 \times (4)^2 \frac{\phi^3}{(1-\phi)^2}$
RT6	5 ≤ FZI < 7	6	$k = 1014 \times (6)^2 \frac{\phi^3}{(1-\phi)^2}$
RT7	7 ≤ FZI	12	$k = 1014 \times (12)^2 \frac{\phi^3}{(1-\phi)^2}$

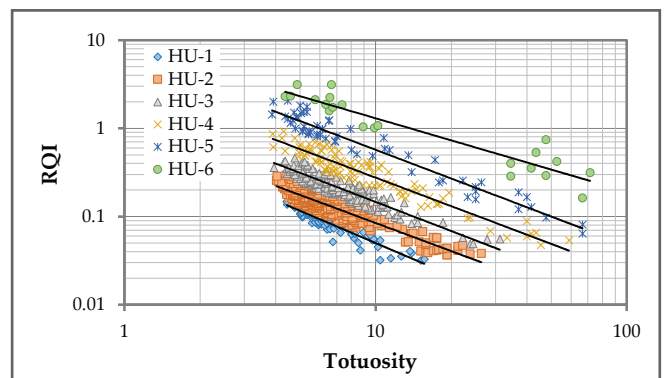
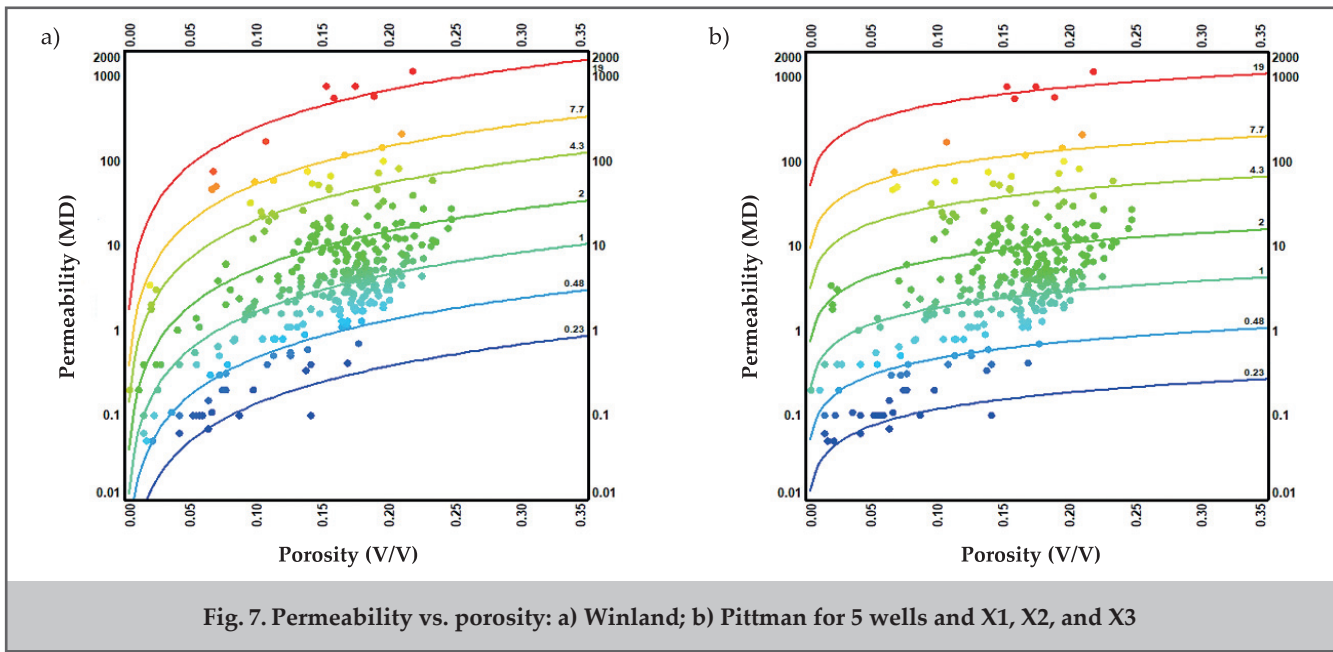
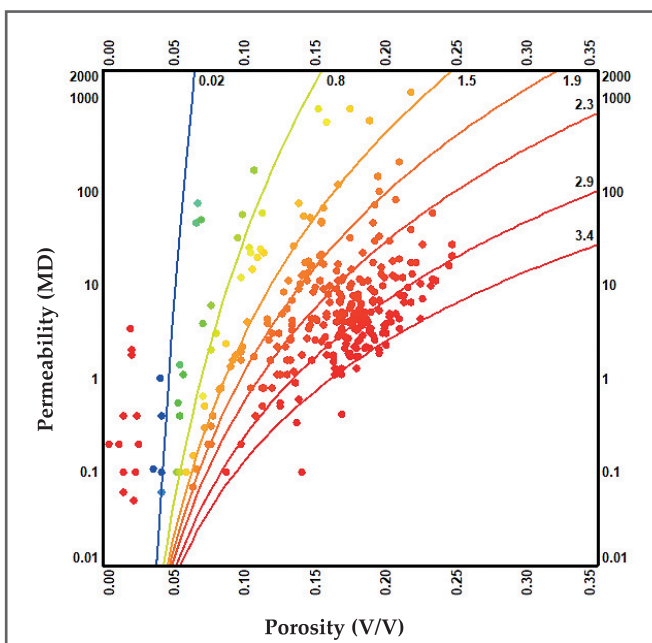


Fig. 6. RQI vs Tortuosity for 5 wells and all units



Rock type	Range of $R_{35}$	$R_{35}$ average	$k-\phi$ formula
RT1	$0.3 > R_{35} > 0.15$	0.23	$K_{air} = 10^{-1.245} \times (0.23)^{1.7} \phi^{1.47}$
RT2	$0.3 \leq R_{35} < 0.55$	0.48	$K_{air} = 10^{-1.245} \times (0.48)^{1.7} \phi^{1.47}$
RT3	$0.55 \leq R_{35} \leq 1$	1	$K_{air} = 10^{-1.245} \times (1)^{1.7} \phi^{1.47}$
RT4	$1.5 \leq R_{35} < 4$	2	$K_{air} = 10^{-1.245} \times (2)^{1.7} \phi^{1.47}$
RT5	$4 \leq R_{35} < 6$	4.3	$K_{air} = 10^{-1.245} \times (4.3)^{1.7} \phi^{1.47}$
RT6	$6 \leq R_{35} < 8$	7	$K_{air} = 10^{-1.245} \times (7)^{1.7} \phi^{1.47}$
RT7	$8 \leq R_{35} < 20$	19	$K_{air} = 10^{-1.245} \times (19)^{1.7} \phi^{1.47}$

Rock type	Range of RFN	RFN average	$k-\phi$ formula
RT1	$0.03 > RFN$	0.02	$k = 10^{30} \times \phi^{22.76}$
RT2	$0.03 \leq RFN < 1.5$	0.8	$k = 10^{10} \times \phi^{9.47}$
RT3	$1.5 \leq RFN < 1.7$	1.5	$k = 10^{7.67} \times \phi^{7.21}$
RT4	$1.9 \leq RFN < 2$	1.9	$k = 10^{6.43} \times \phi^{6.35}$
RT5	$2 \leq RFN < 2.5$	2.3	$k = 10^{5.43} \times \phi^{5.67}$
RT6	$2.5 \leq RFN < 3$	2.9	$k = 10^{4.21} \times \phi^{4.83}$
RT7	$4 \leq RFN$	3.4	$k = 10^{3.37} \times \phi^{4.26}$



**Fig. 8. Permeability vs. porosity, Lucia chart for 5 wells and X1, X2, and X3 units**

diagenesis processes. To verify our proposed hydraulic flow unit model, we collected core data and well logs from four cored wells in the x field, with well-4 serving as the reference well, in order to enhance the reservoir description and detect important patterns in the x formation. The core samples were distributed equally throughout all of x1's sub-units, and the observed porosity and permeability have been corrected for overburden. Over x1 unit (fig. 9) shows a summary of normalized well logs from the study region's main key well Well-4; the findings reflect k-calculated (red dash line) by FZI vs. k-core (blue dot point). Correlations such as those in Eq. 3 capture the overall trend. Notably, five extreme values of permeability (between 50 and 100 md) do not agree well, which is most likely due to the presence of fractures or vugs in the rock unit.

Therefore, in (fig. 10) may be utilized in the same way as FZI, core samples that lie on the same straight line on this plot have comparable properties and can be considered part of the same flow unit. Individual flow units may be estimated using IF to get the free-fluid index and the average value of irreducible water saturation using the following formula. Table 4 summarizes the findings obtained from the correlations and equations discussed previously.

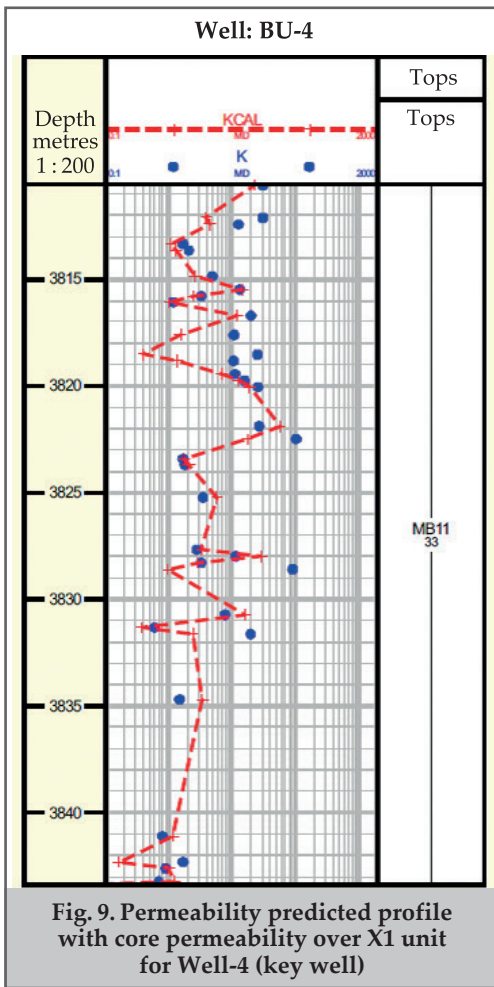
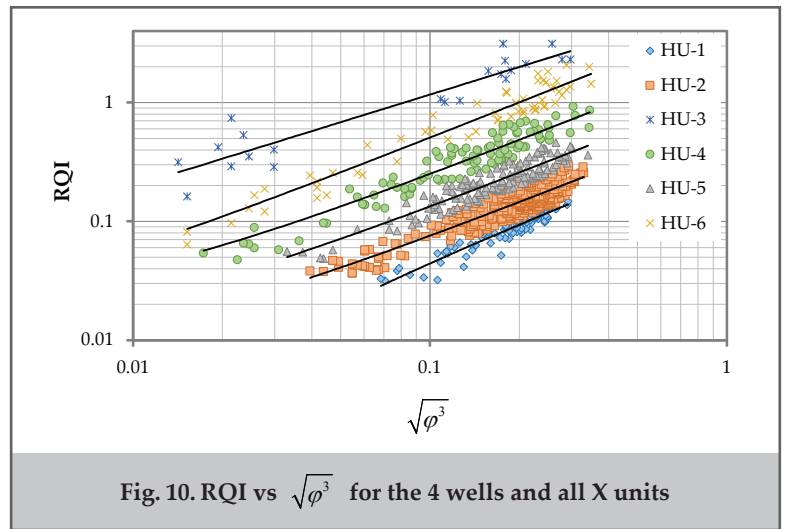


**Table 4**

**The constants from above equations and plots**

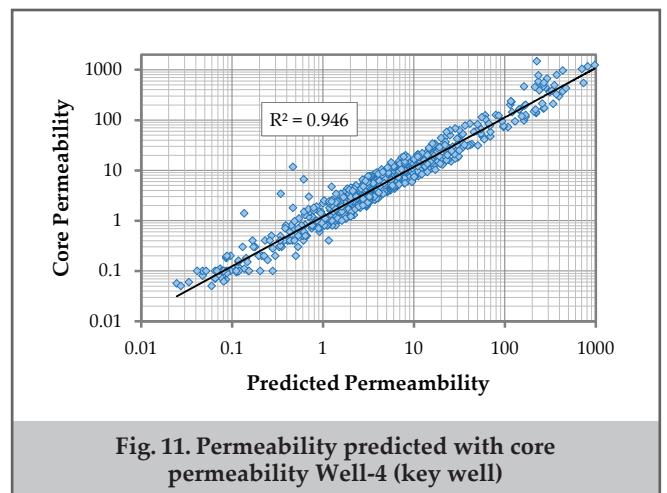
Flow Unit	$\bar{\phi}$	$FFI = (1 - S_{wir})\bar{\phi}$	$C_{pp} = I_F \left( \frac{\bar{\phi}}{FFI} - 1 \right)$	$C_{cd} = \log \left( \frac{C_{pp}}{0.0314} \right)$
1	0.164	0.139289815	0.155294118	1.388450715
2	0.168	0.142489781	0.202941176	1.620881051
3	0.151	0.128290823	0.308823529	1.985561468
4	0.116	0.098266071	0.698823529	2.694875742
5	0.116	0.098747826	1.309411765	3.240293181
6	0.085	0.072310714	2.405294118	3.768477082



The figures 11 and 12 demonstrate how the coates and Denoo method provides good results for projected permeability in all units of the main well (Well-4), as well as how adding water saturation to the porosity-permeability relationship improves the correlation coefficient ( $R_2=0.946$ ). Although several empirical correlations have been suggested thus far to assess permeability, their outcomes are typically not suitable in varied contexts. This is thus because the links ignore all the elements influencing permeability and the interactions among these variables. Applying the same correlations to different aquifers and rocks might not provide the same findings as their lithologies and fluids varied. Though most of Iraq's deposits are carbonate rocks, we still know little about their petrophysical characteristics.

The model would be first trained zone by zone—that is, on X1, X2, X3, and X7. The second step would then run concurrently for the training data for the offset wells on all units. Then, by using the model on the well without initially incorporating the reference wells first, one should compare whether circumstance is superior in forecasting permeability. Investigating error metrics might assist one to better understand the generalizing capability of the model.

The three wells holding the statistics for the units X1 and X2 comprise 512 samples overall. The four wells for X1 and X2 will house model logs- and the source data Geolog 19 Software needs to create the models from. Crossplots and histograms illustrating the relationships among the modeled logs are shown in (fig. 13). For units X1 and X2 these are the histograms, permeability crossplots, and well logs. These crossplots demonstrate how two logues interact and how

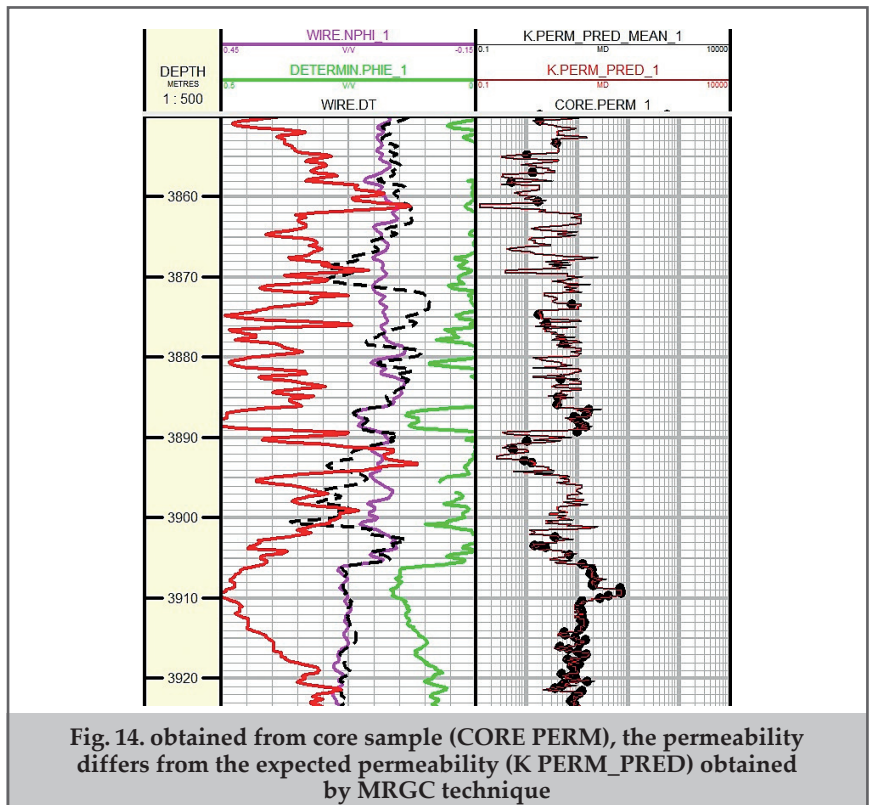
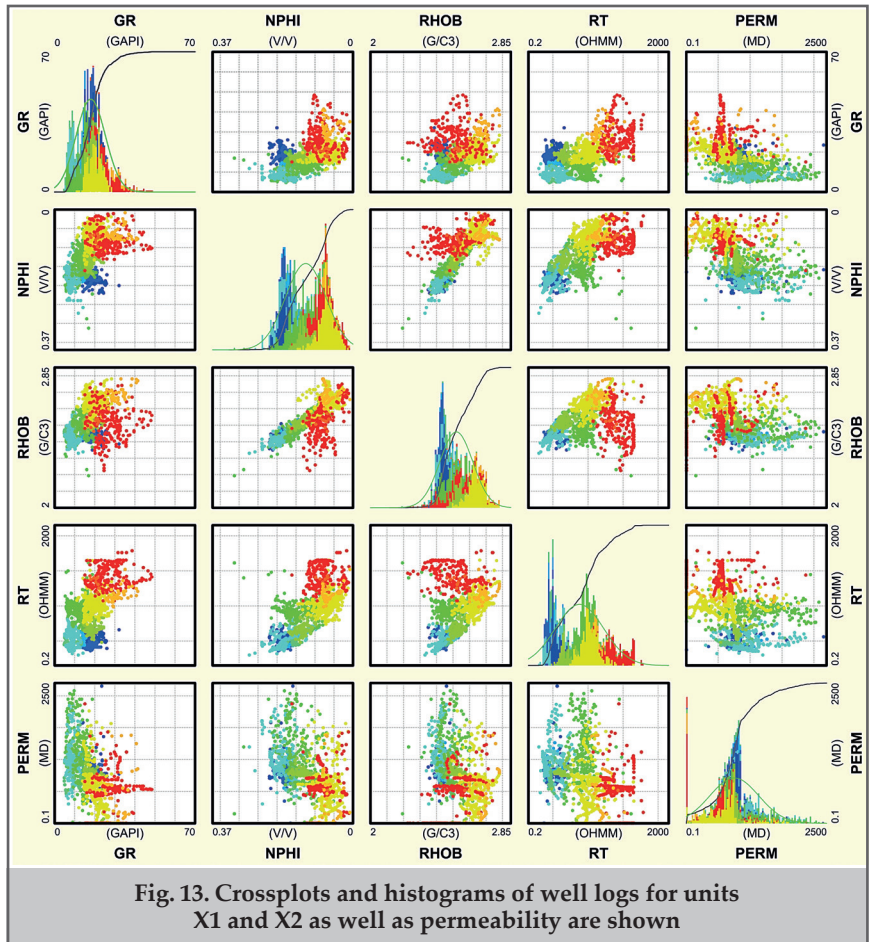
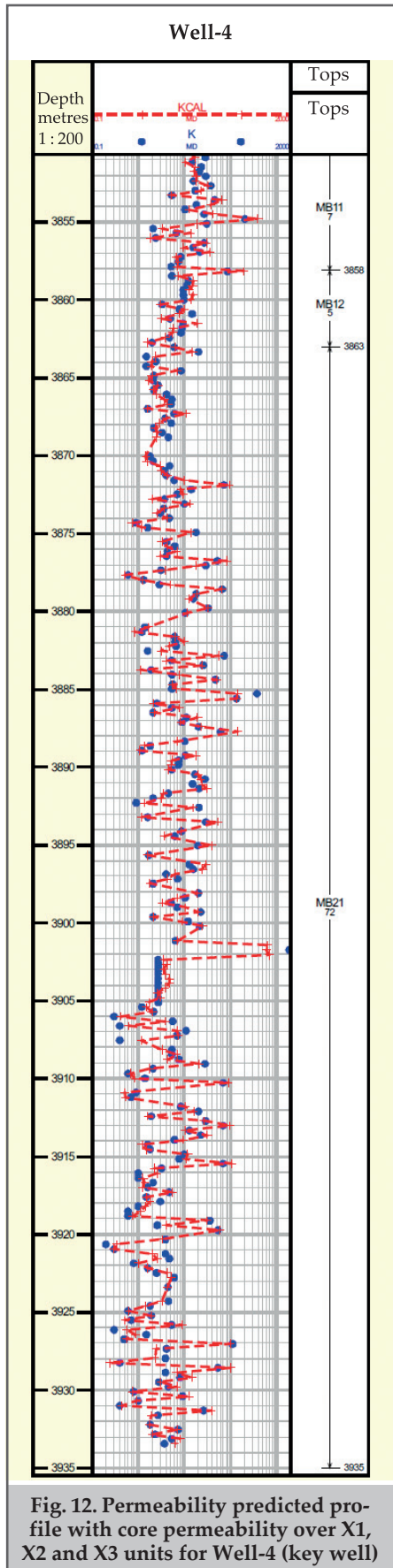


that can suggest particular rock characteristics including permeability. For every log, the histograms provide the value frequency distribution. This helps us to estimate the pool's value range and dispersion. Crossplots can assist in data pattern and outlay identification. The crossplot demonstrate how log is connected and how that relationship could expose particular rock feature including permeability.

The histograms reveal the frequency distribution of the values for every log, therefore providing us with a concept of the pool's range and spread of values. Histograms and crossplots let you identify data outlays and trends. Since every data point indicates a distinct depth in the well, the crossplot demonstrate the relationships between two log

values. For example, a crossplot of NPHI versus RHOB indicates a strong positive association; generally, larger values of NPHI are connected to higher values of RHOB. This link will enable you to determine the density and porous nature of the production. This helps you to understand the appearance of

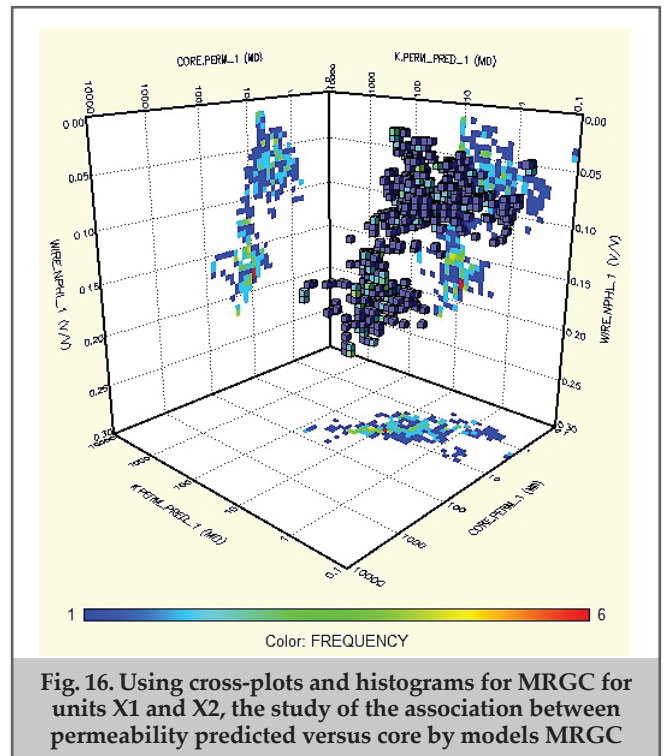
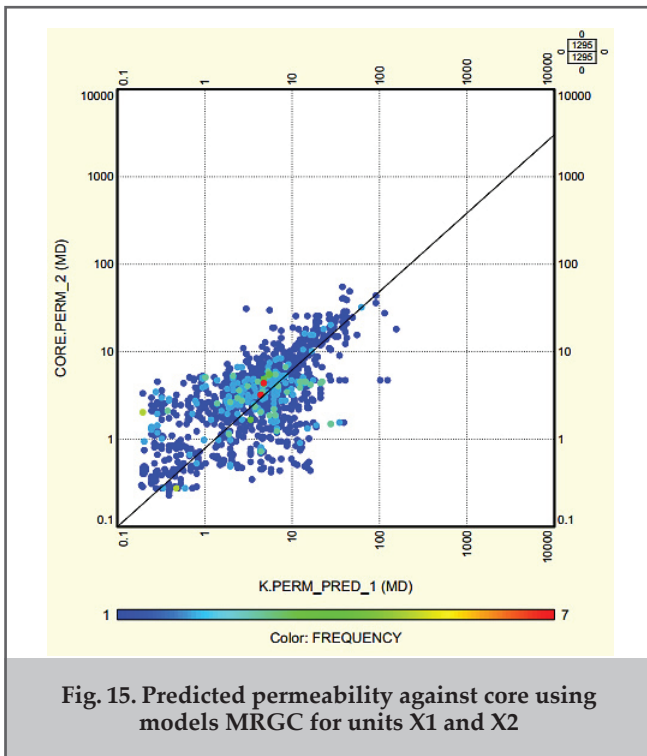
the tank and the possible issues with its purpose. a tiny collection of dots in the crossplot of porosity and permeability, for example, might exhibit a zone with high permeability ideal for output. Figure 14 designed facies X1 and X2. This is the result of automatically grouping depending on the



facies characteristics of the cluster model the values of the learning data. Found usually consists of one or more groups. Figure 14 is most imaginatively produced from our past. For facings there is a name, shade, and fill pattern assigned. Once a cluster model is built, the computer generates rather effective faces for each group. Our investigation of the four MRGC-suggested areas – which comprised 20, 21, 23, and 25 facies – using weighted logs and increased trustworthy probability resulted in the best cluster comprising of 15 facies. Although minimum data should be used to minimize processing times and memory, the forecasts are more accurate the larger the cluster is even if running the models takes time

and requires a strong processor. Out of the 20 and 25 cluster facies, the 20 cluster possessed the most logically exact, precisely projectable permeability.

Using the same interval and unit as X1 and X2, the data is sent to the offset well to forecast permeability after the correct grouping and facies processing model is selected. Three separate validation model results – derived from the T-test, MAE, and RMSE – are presented in table 2. With a larger correlation coefficient ( $R_2=0.96$ ) and a smaller root-mean-squared error (RMSE=40.5), the MRGC model stands out among the others as it estimates values more precisely than the real values as shown in figures 15 and 16.



### Conclusions

This study has provided important insights into the characterization and calculation of permeability in the X formation, a carbonate reservoir. We were able to classify the reservoir into separate rock groups and build robust petrophysical models by employing advanced approaches such as the FZI and ML methodologies, as well as rigorous data analysis of core samples. The intricacies of carbonate rock characteristics, as well as the problems of estimating permeability, underscore the significance of using a variety of approaches and correct datasets. Our investigation led to the following main conclusions:

1. The FZI technique classified the X reservoir into seven groups, each representing a different kind of rock. Each type of rock has a comparable porosity and similar characteristics, which may be utilized to partition the reservoir.
2. The regular and special core analysis data, as well as the core description data, are used as the «real data» for calibrating petrophysical models. We collected, described, and evaluated over four wells.
3. Carbonate rocks have complex and varied pore structures that can result in significant dispersion and poor correlation on the permeability vs. porosity plot. Therefore, when calculating the permeability of carbonate rocks, it is preferable to utilize more than one relationship between porosity and permeability to accurately depict the rock types.
4. The permeability-porosity correlations for X formation, a carbonate reservoir in the investigated field, were calculated using several HU'S systems and Reservoir Quality Index (RQI) ideas. Notably, these methods are based on certain assumptions, such as the rock being homogeneous and isotropic, which may not hold in all situations; therefore, it is important to exercise caution when applying these equations to real-world issues. In addition, accurate data and a description of the rock are required to apply these methods and interpret the results.

5. Permeability estimates are sometimes poor since numerous factors influence it concurrently. Using the same relationships would not allow one to attain the expected findings as not all reservoirs and strata have the same rock types and fluid.
6. Permeability estimation of the X formation using a two-step model grounded on training data. With just three wells and 512 samples, the first case performed better than the second instance – which contained 1322 samples – in terms of permeability. Once a cluster model is developed, the program creates faces for every group really well. This rapidly generates the cluster model depending on the grouping of the learning data values. The predictions can be more accurate the more clusters exist. Two times this occurred, and by identifying sites with 20, 21, 23, and 25 cluster facies, the MRGC model outperformed the others.

### References

1. Al-Yaseri, A. Z., Sattam, M., Alameedy, U. (2013). Improve permeability prediction for one of Iraqi carbonate oil reservoir. *Journal of University of Babylon*, 21(February), 1289–1300.
2. Alameedy, U., Almomen, A., Abd, N. (2023). Evaluating machine learning techniques for carbonate formation permeability prediction using well log data. *Iraqi Geological Journal*, 56(1D), 175–187.
3. Winland, H., D. (1972). Oil accumulation in response to pore size changes. In: *Field, W., Ed., Amoco Production Research Report, Saskatchewan*.
4. Pittman, E. D. (1992). Relationship of porosity and permeability to various parameters derived from mercury injection-capillary pressure curves for sandstone. *AAPG Bulletin*, 76(2), 191-198.
5. Lucia, F. J. (1999). Carbonate reservoir characterization. *Berlin Heidelberg: Springer*.
6. Alameedy, U., Farman, G., Al-Tamemi, H. (2023). Mineral Inversion approach to improve Ahdeb Oil Field's mineral classification. *Iraqi Geological Journal*, 56(2B), 102–113.
7. Corbett, P. W. M., Potter, D. (2004). Petrotyping: A basemap and atlas for navigating through permeability and porosity data for reservoir comparison and permeability prediction. SCA2004-30. In: *The International Symposium of the Society of Core Analysts, January*.
8. Kurniawan, D. H., Winardi, S., Anggara, F. (2021). Linking between sedimentary facies and petrophysical rock type: A case study. *IOP Conference Series: Earth and Environmental Science*, 789(1), 012077.
9. Mohebian, R., Bagheri, H., Kheirollahi, M., Bahrami, H. (2021). Permeability estimation using an integration of multi-resolution graph-based clustering and rock typing methods in an Iranian carbonate reservoir. *Journal of Petroleum Science and Technology*, 11(3), 49–58.
10. Rushing, J. A., Newsham, K. E., Blasingame, T. A. (2008, February 10). Rock typing — keys to understanding productivity in tight gas sands. SPE-114164-MS. In: *SPE Unconventional Reservoirs Conference, Keystone, Colorado, USA*.
11. Amraei, H., Falahat, R. (2021). Improved ST-FZI method for permeability estimation to include the impact of porosity type and lithology. *Journal of Petroleum Exploration and Production Technology*, 11(1), 109–115.
12. Bear, J. (1972). Dynamics of fluids in porous media. *Elsevier*.
13. Ebanks, W. J. (1987). The flow unit concept—an integrated approach to reservoir description for engineering projects. *American Association of Petroleum Geologists Bulletin*, 71, 551–552.
14. Hearn, C. L., Ebanks, W. J., Tye, R. S., Ranganathan, V. (1984). Geological factors influencing reservoir performance of the Hartzog Draw Field, Wyoming. *Journal of Petroleum Technology*, 36(08), 1335–1344.
15. Gunter, G. W., Finneran, J. M., Hartmann, D. J., Miller, J. D. (1997, October 5). Early determination of reservoir flow units using an integrated petrophysical method. SPE-38679-MS. In: *SPE Annual Technical Conference and Exhibition, October 5–8*.
16. Schmalz, J. P., Rahme, H. D. (1950). The Variation of waterflood performance with variation in permeability profile. *Producers Monthly*, 15(No. 9), 9–12.
17. Law, J. (1944). Statistical approach to the interstitial heterogeneity of sand reservoirs. *SPE Transactions*, 155(01), 202-222.
18. Dykstra, H., Parsons, R. L. (1950). The prediction of oil recovery in waterflood. Secondary recovery of oil in the United States. *American Petroleum Institute (API)*.
19. Warren, J. E., Price, H. S. (1961). Flow in heterogeneous porous media. *SPE Journal*, 1(03), 153–169.
20. Tiab, D., Donaldson, E. C. (2015). Petrophysics: theory and practice of measuring reservoir rock and fluid transport properties (4th Ed.). *Gulf Professional Publishing - Elsevier*.
21. Amaefule, J. O., Altunbay, M., Tiab, D., et al. (1993, October 3). Enhanced reservoir description: using core and log data to identify hydraulic (flow) units and predict permeability in uncored intervals/wells. SPE-26436-MS. In: *The SPE Annual Technical Conference and Exhibition, Houston, Texas*.
22. Coates, G., Denoo, S. (1981). The producibility answer product. The technical review. *Schlumberger*.
23. Mahdy, A., Zakaria, W., Helmi, A., et al. (2024). Machine learning approach for core permeability prediction from well logs in sandstone reservoir, Mediterranean Sea, Egypt. *Journal of Applied Geophysics*, 220, 105249.
24. Kumar, V., Banerjee, A., Roy, K. (2024). Breaking the barriers: machine-learning-based c-RASAR approach for accurate Blood–Brain barrier permeability prediction. *Journal of Chemical Information and Modeling*, 64(10), 4298–4309.

25. Ita, K., Roshanaei, S. (2024). Artificial intelligence for skin permeability prediction: deep learning. *Journal of Drug Targeting*, 32(3), 334–346.
26. Khalid, M. S., Mansour, A. S., Desouky, S. E.-D. M., et al. (2024). Improving permeability prediction via machine learning in a heterogeneous carbonate reservoir: application to Middle Miocene Nullipore, Ras Fanar field, Gulf of Suez, Egypt. *Environmental Earth Sciences*, 83(8), 244.
27. Kang, Q., Li, K.-Q., Fu, J.-L., Liu, Y. (2024). Hybrid LBM and machine learning algorithms for permeability prediction of porous media: A comparative study. *Computers and Geotechnics*, 168, 106163.
28. Davari, M. A., Senemari, S., Alimoradi, A., Safavi, S. J. (2024). Permeability prediction from log data using machine learning methods. *Journal of Petroleum Geomechanics*, 7(3), 1-17.
29. Kumar, V., Banerjee, A., Roy, K. (2024). Breaking the barriers: Machine-learning-based c-RASAR approach for accurate blood–brain barrier permeability prediction. *Journal of Chemical Information and Modeling*, 64(10), 4298–4309.
30. Aftab, N., Masood, F., Ahmad, S., et al. (2024). An optimized deep learning approach for blood-brain barrier permeability prediction with ODE integration. *Informatics in Medicine Unlocked*, 48, 101526.
31. Zhao, J., Wang, Q., Rong, W., et al. (2024). Permeability prediction of carbonate reservoir based on nuclear magnetic resonance (NMR) logging and machine learning. *Energies*, 17(6), 1458.
32. Ita, K., Prinze, J. (2024). Machine learning for skin permeability prediction: random forest and XG boost regression. *Journal of Drug Targeting*, 32(1), 57–65.